Available online at www.sciencedirect.com

SciVerse ScienceDirect

Acta Materialia 60 (2012) 3402–3414

Acta MATERIALIA

www.elsevier.com/locate/actamat

In situ TEM observations of reverse dislocation motion upon unloading in tensile-deformed UFG aluminium

Frédéric Mompiou [a], Daniel Caillard [a,*], Marc Legros [a], Haël Mughrabi [b]

[a] CEMES-CNRS, 29 rue J. Marvig, BP94347, 31055 Toulouse Cedex, France

[b] Department of Materials Science and Engineering, University Erlangen-Nürnberg, Martensstrasse 5, 91058 Erlangen, Germany

Received 15 November 2011; received in revised form 20 February 2012; accepted 25 February 2012

Abstract

Loading–unloading cycles have been performed on ultrafine-grained (UFG) aluminium inside a transmission electron microscope (TEM). The interaction of dislocations with grain boundaries, which is supposed to be at the origin of the inelastic behaviour of this class of materials, differs according to the main character of the dislocation segments involved in pile-ups. Pile-ups are formed by spiral sources and lead to the incorporation of dislocations into grain boundaries (GBs) during loading. Upon unloading, partial re-emission of dislocations from GBs can be observed. Stress and strain measurements performed during these in situ TEM loading–unloading experiments are in agreement with the rather large inelastic reverse strains observed during unloading in loading–unloading tests on bulk macroscopic UFG aluminium specimens.

Keywords: UFG aluminium; Transmission electron microscopy; In situ loading–unloading experiment; Inelastic reverse strain

1. Introduction

Bulk ultrafine-grained (UFG) metals produced by equal channel angular pressing (ECAP) have attracted much attention during the last decade because of their extraordinary strength properties (e.g. [1–3]). As compared to conventional grain (CG) size materials, UFG materials exhibit a much higher flow stress, which can be described by the well-known Hall–Petch law. The origin of this higher strength undoubtedly lies in their higher content of grain boundaries (GBs), which are very efficient obstacles to dislocation motion. Another intriguing property of UFG metals, which is probably related to the first one, is their unusual large inelastic reverse deformation upon unloading, as has been shown some time ago for both UFG copper [4,5] and UFG aluminium [6,7]. In contrast to reference CG materials, which show almost completely elastic unloading behaviour under similar conditions, the UFG metals studied exhibited an inelastic back strain which can be as large as 5×10^{-4} in the case of UFG copper and more than 2×10^{-4} in the case of UFG aluminium. The example shown in Fig. 1 refers to UFG aluminium.

Since the grain size of UFG materials is, typically, a few hundred nanometers, i.e. comparable to the observable foil thickness in transmission electron microscopy (TEM), the ratio of boundary surface to free surface is higher than in CG materials (although generally still smaller than unity). Surface effects should accordingly be reduced, and the inelastic behaviour be at least partly reproduced in in situ TEM experiments. Such experiments have been carried out recently on nanocrystalline Al and Au [8]. In such materials, the very high inelastic back strain has been explained by a heterogeneous distribution of grain size leading to a heterogeneous deformation [3]. However, in the UFG samples discussed here, preliminary experiments indicated that the inelastic back flow should result from another origin, probably related to dislocation–GB interaction and the related deformation-induced internal stresses

* Corresponding author. Tel.: +33 5 62 25 78 72; fax: +33 5 62 25 79 99. *E-mail address:* caillard@cemes.fr (D. Caillard).

1359-6454/$36.00 © 2012 Acta Materialia Inc. Published by Elsevier Ltd. All rights reserved.
doi:10.1016/j.actamat.2012.02.049

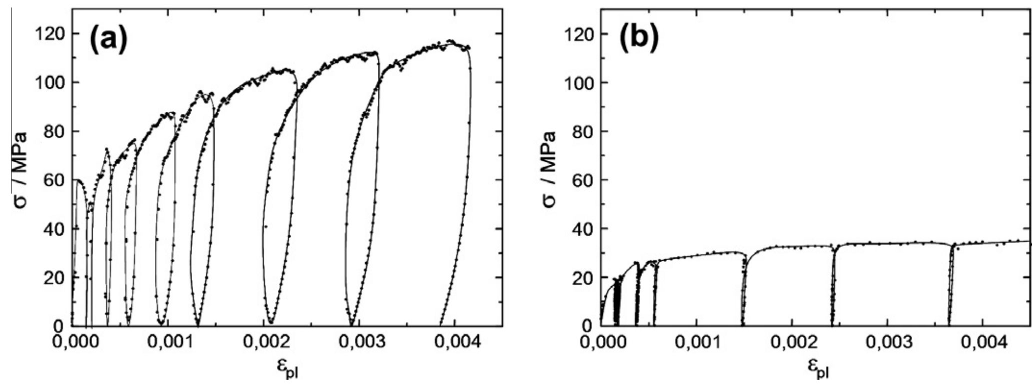

Fig. 1. Tensile microyielding stress–strain curves (plot of stress σ vs. plastic strain ε_{pl}) with repeated unloadings and reloadings: (a) UFG aluminium, as-ECAP; (b) CG aluminium (from Refs. [6,7]).

[9]. Dislocation interaction with low-angle boundaries has been studied in situ a long time ago, in crept Al [10,11]. However, dislocation interactions with high-angle GBs are expected to be different from those with low-angle subgrain boundaries consisting of lattice dislocation networks.

Dislocation–GB interactions have been the subject of a large amount of theoretical and experimental studies, which will not be reported here, but which can be found in the review paper of Priester [12]. In situ straining experiments were performed on a Ge bicrystal by Michaud et al. [13] to observe the insertion of dislocations into GB. In situ annealing experiments were also carried out by Poulat et al. [14] and Couzinié et al. [15] in order to observe the kinetics of relaxation of lattice dislocations inserted in GBs of Ni and Cu. Recently, Chassagne et al. [16] combined in situ TEM and molecular dynamics to study dislocations– twin interactions. However, only particular GBs with low Σ values were studied in these experiments and the elastic interaction forces between dislocations and GB were not determined.

In order to observe the real interaction processes between mobile dislocations and random GBs, more detailed loading–unloading in situ TEM experiments than reported earlier [9] were performed on a UFG aluminium sample produced by ECAP. The results described below are complementary to those already published in our preliminary article [9].

2. Experimental procedure

UFG aluminium of commercial purity with a 300 nm average grain size was obtained by ECAP processing with 8 route B_c passes (die angle 90°), with a rotation of 90° in the same sense around the specimen axis after every pass (courtesy of Johannes May, Erlangen). Rectangular microsamples, of size 3 mm × 1 mm, were prepared by spark cutting, followed by mechanical grinding and electropolishing. They were fixed on a Gatan room-temperature straining device, and strained in a JEOL 2010HC transmission microscope [17]. The fixation was such that the stress could be released without inducing any compression. This latter point is well established because all attempts at compressing microsamples by reversing the sense of straining only resulted in buckling and bending with complete loss of focus in the TEM. The dynamic sequences were recorded by a Megaview III video camera, and analysed frame by frame.

Grain orientations are determined by diffraction experiments. Slip planes are deduced from the direction of slip traces left by moving dislocations at the two surfaces, and from their apparent distances (which give the slip plane inclinations). Burgers vectors are determined by contrast analyses performed during the experiments, and/or deduced from cross-slip observations (Burgers vectors being parallel to the intersection of two different slip planes).

3. Results

3.1. General observations

We noted a slight increase of the average grain size with respect to earlier observations, as a result of the storage of the UFG material during several months at room temperature. The resulting average grain size was ~500 nm. Markedly different behaviours have been observed in the different grains investigated in several samples. The results obtained on three grains, as reported below, are fairly representative of this diversity.

Just after the microsamples are loaded for the first time, only the few grains which contain dislocation sources can deform extensively. Then, slip transfer becomes possible across GBs; as a result all grains are provided with mobile dislocations, and plastic deformation becomes more homogeneous. One consequence of grain sizes smaller than one micron is that the relative deformation generated by a single dislocation becomes appreciable. As a reminder for the following examples, one perfect $a/2[1\,1\,0]$ dislocation ($b = 0.286$ nm) shearing a 570 nm grain leads to a maximum deformation of 5×10^{-4}.

3.1.1. First example

Fig. 2 shows the behaviour of a grain containing a source where – for reasons which are subsequently discussed – no inelastic back flow is observed upon unloading. The grain has a grain size of ~800 nm and is oriented with a $[\bar{1}24]$ direction perpendicular to the foil plane, and a $[611]$ direction parallel to the tensile axis. A dislocation source with anchoring point S rotates anticlockwise and emits a dislocation loop gliding in (111) (slip trace tr_1 in Fig. 2d) and cross-slipping in $(1\bar{1}1)$ (slip traces tr_1–tr_3 in Fig. 3a). Since the dislocation is in contrast with the diffraction vector $g = \bar{1}\bar{1}1$, its Burgers vector is $1/2[\bar{1}01]$. This dislocation is completely inserted in the left GB (contrast d_i, Fig. 2b). Then, no more plasticity is observed during the next few seconds, until Fig. 2c. Fig. 2d and e shows two difference images, obtained by subtracting the contrasts of respectively Fig. 2b and a, and Fig. 2c and b, in which only the changing details are seen in black/white contrast. Fig. 2d (b–a) thus shows the dark contrast d_i of the inserted dislocation, and Fig. 2e (c–b) shows that this contrast (as well as the slip trace) decreases during the following 7 s. Similar absorption processes will be described in the following examples.

Fig. 3 shows the continuation of the loading process, followed by the first unloading test. During loading, the source has emitted two more dislocations, with slip traces tr_2 and tr_3, all inserted into the left GB. It is interesting to note that as a result of various amounts of cross-slip in the $(1\bar{1}1)$ plane, the dislocations intersect the GB at different places 50 nm apart. Then, the sample is unloaded (Fig. 3b and c). No substantial reverse dislocation motion is observed upon unloading, except for the unbowing of the curved arm of the source (arrowed). In particular, none of the inserted dislocations moves back from the left GB.

3.1.2. Second example

The second example again corresponds to the plastic behaviour of a grain containing a source. However, contrary to the previous one, a substantial back flow is observed, as a result of the low amount of cross-slip favouring the formation of short dislocation pile-ups.

The investigated grain is shown in Fig. 4. It exhibits a slightly larger grain size of about 1500 nm. Up to 15 loading–unloading tests have been performed in the observation period of 36 min, during which a dislocation source has emitted 33 dislocation loops, numbered 1 to 33. The grain is oriented with a [001] direction perpendicular to

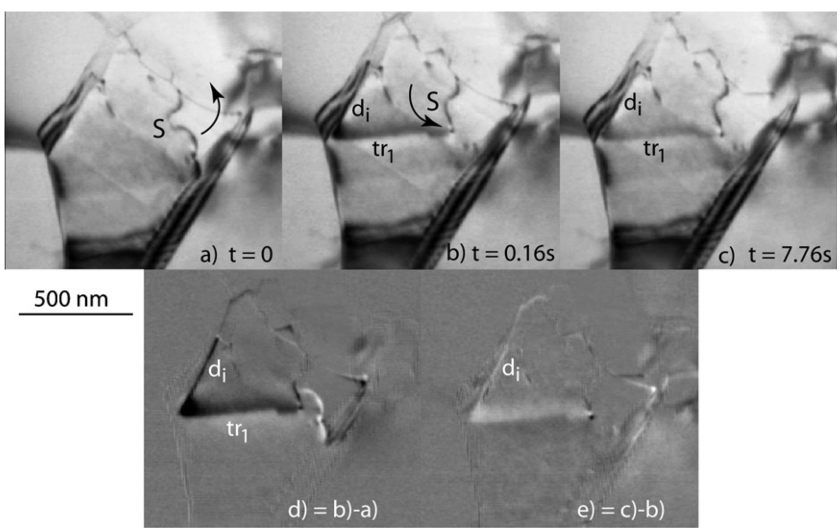

Fig. 2. (a–c) Single-armed dislocation source (anchoring point S) emitting a near-screw dislocation loop (slip trace tr_1), which enters the left GB in d_i. Diffraction vector $\bar{1}\bar{1}1$, vertical tensile direction. (d) The difference image (b–a) shows the contrast of d_i just after insertion in the GB. (e) The difference image (c–b) shows the decrease of the contrast with time.

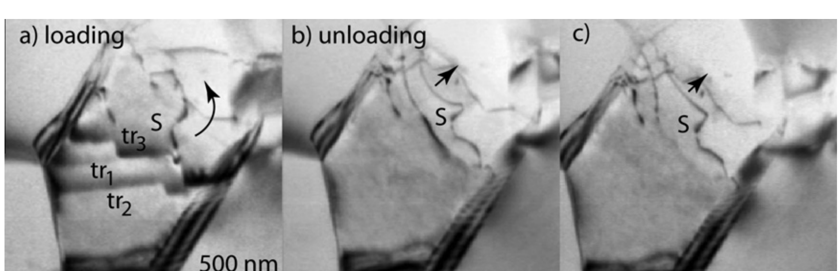

Fig. 3. Continuation of the sequence of Fig. 2. (a) Two additional dislocations are emitted and inserted in the left GB (traces tr_2 and tr_3) during loading. (b and c) No back motion is observed during unloading, except for the unbowing of the dislocation arm connected to the source (the direction of reverse motion is arrowed).

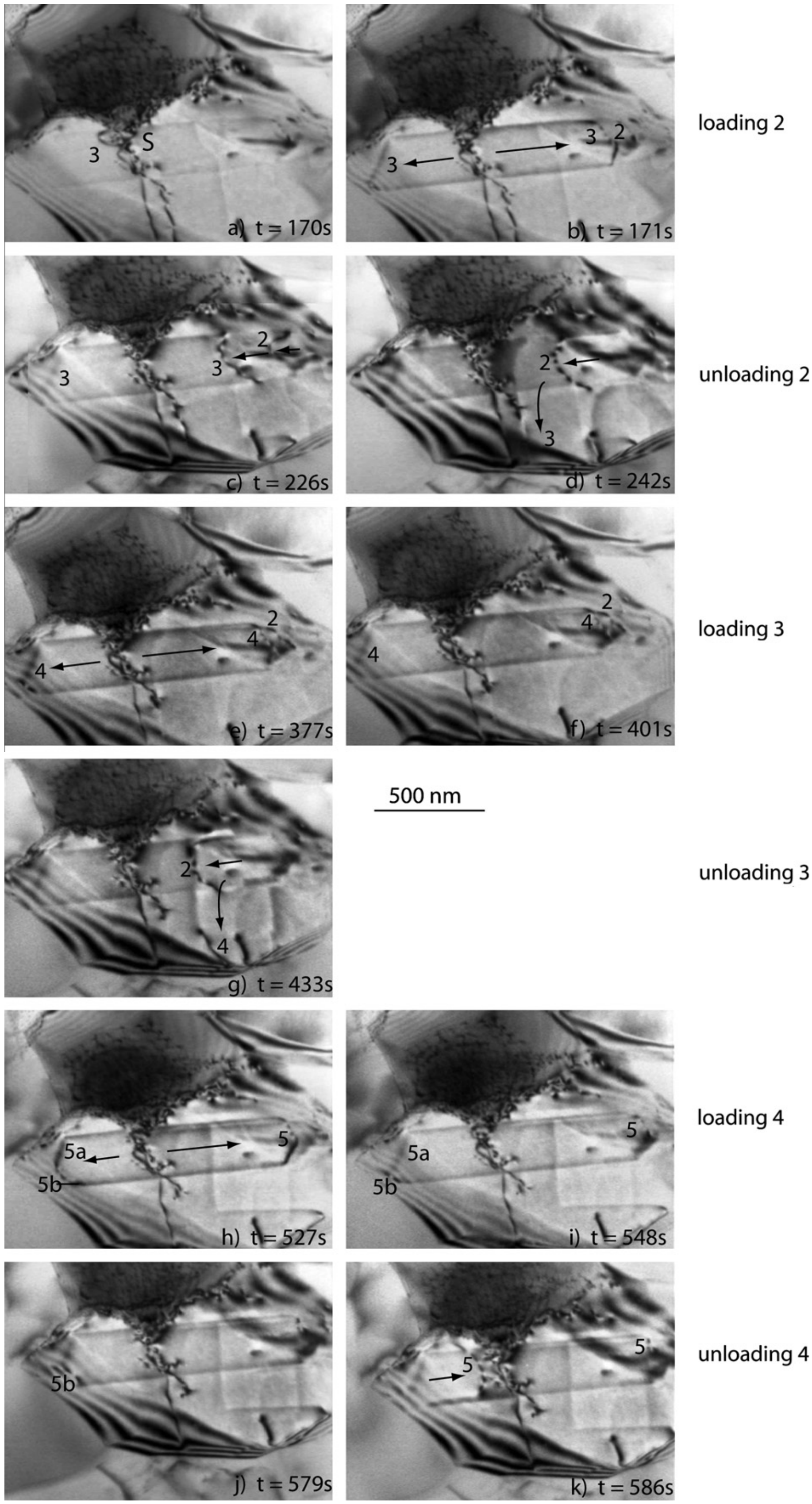

Fig. 4. Series of loading–unloading experiments, in a grain containing a source (S) emitting near-edge segments. Diffraction vector 020, vertical tensile direction. Note the disappearing of dislocations 3 and 4 in the left GB, and the back motion upon unloading of dislocations 2, 3 (piled up against the right GB), and 5 (partly inserted in the left GB).

the foil plane, and a [3 2 0] direction parallel to the straining axis. The source (anchoring point S) emits dislocations gliding in $(\bar{1}\,\bar{1}\,1)$ planes. Since these dislocations are visible with $g = 020$, and out of contrast for $g = 200$, and since they tend to cross-slip in $(1\,\bar{1}\,1)$ (see Fig. 4g), their Burgers vector is 1/2[0 1 1]. The left and right GB planes are close to $(\bar{1}\,0\,1)$, in such a way that inserting dislocations have a nearly 60° character.

Fig. 4 starts with the second loading step of the observation period, at $t = 170$ s (Fig. 4a), where dislocation 1 has already disappeared. The two first loading–unloading sequences of this figure (Fig. 4a–d and e–g, respectively) show an inelastic back flow at the right-side GB, whereas the third one (in Fig. 4h–k) shows another – but different in nature – backflow at the left-side GB. At the beginning of the sequence, at $t = 171$ s (Fig. 4b), the third observed dislocation loop, noted 3, is emitted by the source S. Because this loop is truncated by the two foil surfaces, it appears as two segments ending at the surfaces, and moving in opposite directions. The left segment is immediately absorbed in the left GB, whereas the right one piles up against another previously emitted dislocation (noted 2), in front of the right GB. Note that dislocation 2 is not yet inserted in the right GB, probably as a result of a high repulsive stress. Note also that the contrast of the dislocation in the left GB becomes much broader than in the crystal, and that this contrast vanishes with time (Fig. 4b and c). During the following stress release, two backward dislocation motions are observed, of dislocations 3 and 2 (Fig. 4d). Note that the backward motion of dislocation 3 involves cross-slip in $(1\,\bar{1}\,1)$. The corresponding backward flow is much larger than in Fig. 3 above.

The second loading step starts at $t = 377$ s (Fig. 4e). It involves the emission of dislocation loop no. 4, which again disappears at the left GB (Fig. 4e–g), and piles up against dislocation 2 at the right one. Both dislocations 2 and 4 move backward and cross-slip in $(1\,\bar{1}\,1)$ upon unloading at $t = 433$ s (Fig. 4g).

The third loading step involves the emission of dislocation loop no. 5 (Fig. 4h and i). Interestingly, this dislocation is only partly inserted in the left GB (segment 5a), and thus partly still outside (segment 5b), which induces a different behaviour upon unloading. As a matter of fact, the segment 5b is seen to move back at $t = 579$ s (Fig. 4j), and to pull the whole dislocation out of the GB and back to the source, at the end of the sequence (Fig. 4k).

The origin of the large inelastic back flow can be deduced from the inspection of Fig. 5. In this figure, the source S is at rest, and all the previously inserted dislocations have been absorbed in the two opposite GBs. Two anomalous contrasts can, however, be seen at the insertion places: a broad and large dark contrast in the right GB, in A, and a distortion of the fringe pattern of the left GB, in B. They reveal strong lattice distortions and associated internal stresses, which are sufficient to initiate the observed back flow.

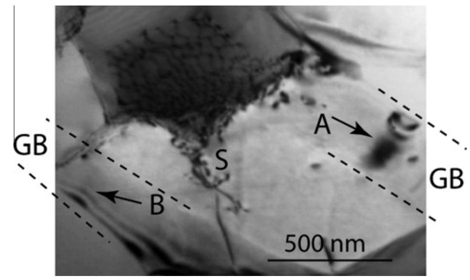

Fig. 5. Contrasts of the dislocations emitted by the source S, and absorbed by the two opposite GBs, in A and B.

3.1.3. Third example

After several per cents of deformation, all grains are plastically deformed, including those not containing dislocation sources. This results from the transfer of dislocations through GBs, in zones of very large stress concentration (see an example of GB crossing in Fig. 6). Fig. 7 shows such a grain, of 500 nm size, in which two loading–unloading experiments with substantial inelastic backflow have been performed. The foil normal is $[\bar{1}\,1\,2]$ and the tensile axis is parallel to [2 0 1]. One dislocation ($b = 1/2[0\,\bar{1}\,1]$) moves back and forth in the directions arrowed. It is first extracted from the left GB (Fig. 7a), then glides in a (1 1 1) plane with almost horizontal slip traces (Fig. 7b), and goes into the opposite GB (Fig. 7c). During the unloading, the curvature and the motion change their direction, and the dislocation moves back to the left GB (Fig. 7d–f). The same type of motion is repeated after a second loading–unloading (Fig. 7g–l). Note in addition the partial extraction of another dislocation from the right GB upon unloading, at $t = 2480$ s (Fig. 7f).

This sequence indicates that fully reversible dislocation motion is possible between two opposite GBs, and that back motion upon unloading looks similar to forward motion. It is also important to note that the mobile dislocation is never completely inserted in the GBs, in such a way that the non-inserted segments can pull out the whole dislocation and initiate the back motion.

3.1.4. Summary of general observations

The global dislocation behaviour observed in Figs. 2–7 can be summarized as follows:

(i) Dislocations inserted in GBs have a rapidly vanishing broad contrast, of life time shorter than a few minutes (Fig. 2, and Fig. 4, left side).
(ii) The accumulation of dislocations in GBs generates lattice distortions and a corresponding stress field.
(iii) Dislocations piling up in front of GBs (Fig. 4, right side), and dislocations partly inserted in GBs (Fig. 4, left side and Fig. 7), can move back when the applied stress is released. On the contrary, completely inserted dislocations remain stuck in GBs (Fig. 2, and Fig. 4, left side).

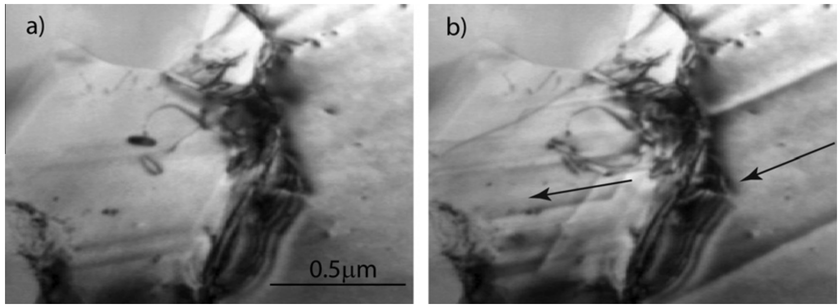

Fig. 6. Slip transfer across a grain boundary. (a) Two grains separated by a GB are in contrast simultaneously. (b) After 1/25 s, slip traces have been left on both sides by dislocations moving from right to left.

This can be interpreted by the formation of various kinds of stress fields in GBs. Indeed, although individual dislocations dissolve in GBs in a few tens of seconds, or in a few minutes, their long-range stress field should remain sufficient to repel other dislocations. When intensive cross-slip takes place (i.e. when dislocations have a large screw component, in the case of Figs. 2 and 3), the repulsion force of the first inserted dislocations scatters the dislocations emitted subsequently by the source in a wide area of the GBs. Since this cannot induce large stress concentrations, the following approaching dislocations are not significantly repelled; as a result they are completely inserted, and too difficult to extract upon unloading. On the contrary, when cross-slip is suppressed (i.e. when dislocations have a large edge component, in the case of Figs. 4 and 5), all dislocations emitted by sources reach GBs at the same place, which builds large repulsive stress concentrations. Then, the following dislocations pile up in front of GBs, or at least do not insert completely; as a result their back motion upon unloading is much easier.

Large stress concentrations are the result of a competition between two different processes: the accumulation of inserted dislocations, and the decrease of their stress field as a function of time, probably by diffusion, at least for non-screw dislocations.

Quantitative measurements have been carried out at different steps of the deformation of the second grain (Figs. 4 and 5), in order to estimate the various driving forces at the origin of the back flow.

3.2. Local stress measurements

Fig. 8a shows a curved dislocation loop close to the source S of Fig. 4, after geometrical corrections compensating for slip plane inclination. It has an elliptical shape with long axis parallel to the screw orientation, which can be compared with theoretical shapes computed at various stresses, using the software DISDI [18]. The best fit is obtained for a resolved shear stress $\tau_f \approx 45$ MPa. This corresponds to the forward stress necessary to source operation. Fig. 8b and c shows the same kind of measurement, on dislocations curved in the opposite direction during unloading. The corresponding stress is $\tau_b \approx 23$ MPa on the left side (Fig. 8b) and $\tau_b \approx 20$ MPa on the right one (Fig. 8c). The latter value corresponds to the internal backward stress at the origin of inelastic flow. Considering that the back stress opposes the applied stress during loading, the local applied stress τ_a should thus be equal to the forward stress (the driving stress for source operation), plus the backward one (considered positive), namely $\tau_a = \tau_f + \tau_b \approx 66$ MPa. This value is close to the macroscopic flow stress at $\varepsilon > 4 \times 10^{-3}$ ($\sigma \sim 110$ MPa) multiplied by an average Schmid factor of 0.45, which shows that the strengthening effect of the ECAP process is well reproduced in the microsample.

3.3. Decrease of dislocation contrast in GBs

As already shown in Figs. 2 and 4, dislocations inserted in GBs have a broad contrast progressively vanishing with time. This "spreading phenomenon" has already been observed by Pumphreys and Gleiter [19], Varin [20] Valiev et al. [21], Swiatnicki et al. [22], Kwiecinski and Wyrzykowski [23], and Priester [12]. It can be described by an increase of dislocation core width, or by a decomposition of the lattice dislocation into partial GB dislocations with Burgers vectors too small to be resolved. Two spreading phenomena are shown in Fig. 9: one for an individual dislocation (already seen in Fig. 4 between $t = 527$ s and $t = 548$ s), and one for another dislocation of the same type, emitted by the same source, and entering the GB at the same place, but pushed by a pile-up of two dislocations. The corresponding contrast intensities, plotted as a function of time, exhibit a progressive decrease with respective characteristic times (given be the slope at the origin) of 9 s and 3.5 s. Since the two events are geometrically similar, it is inferred that the spreading is enhanced by the repulsive stress concentration of the pile-up.[1] The curve of Fig. 9 is similar to that obtained by Kwiecinski and Wyrzykowski [23], showing the fraction of grain boundaries still containing dislocations after annealing during a given time t, and fitted by an equation of the type $C = A–B \ln t$, where C is the contrast

[1] Since the spreading mechanism involves only short-range atomic displacements, the spreading rate is assumed to be only weakly dependent on the length of the inserted dislocation.

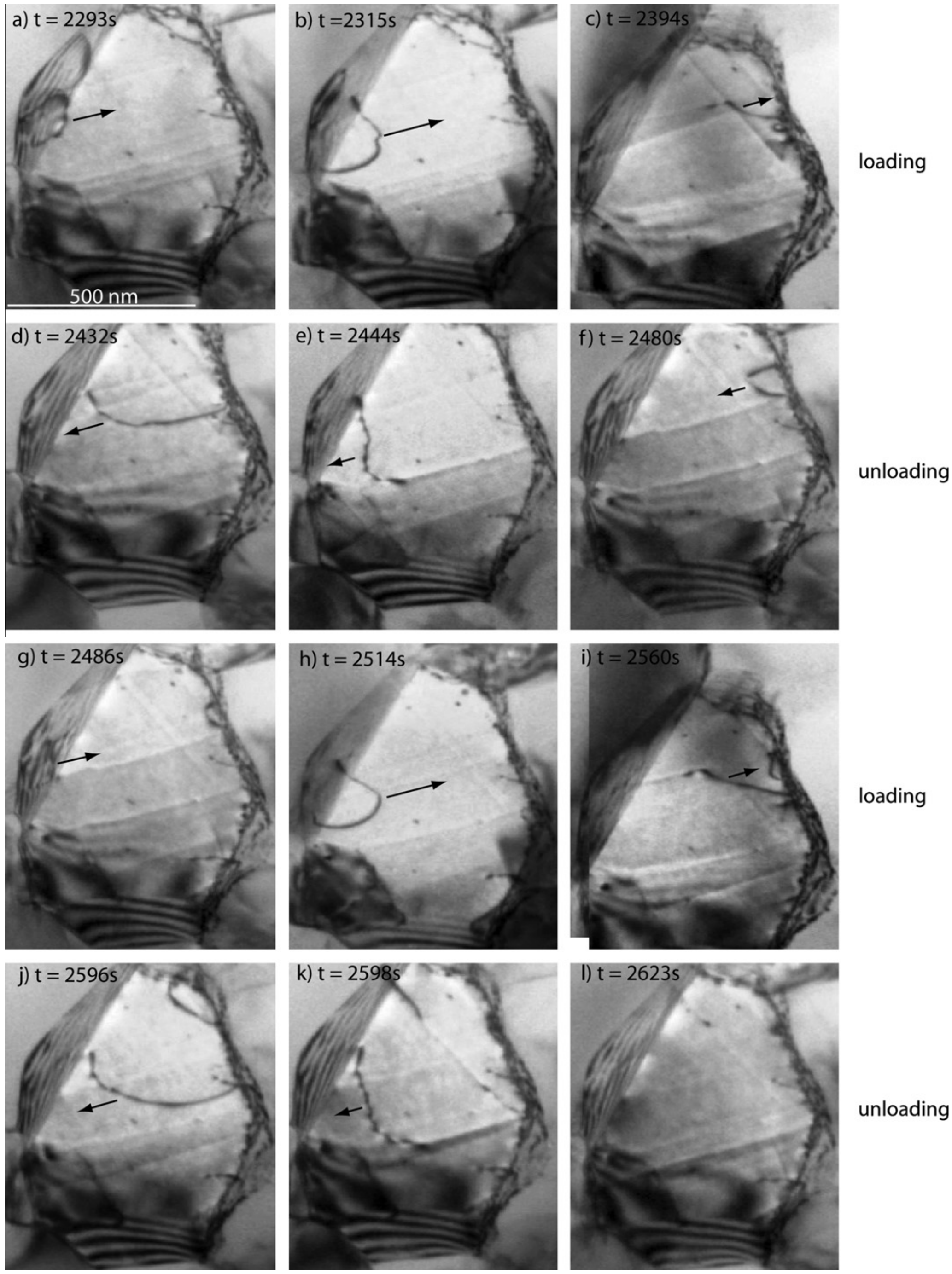

Fig. 7. Series of loading–unloading experiments, in a grain with no source. Note the back and forth motion of a dislocation (arrows) between the two opposite GBs.

intensity, A and B are constants. The characteristic time is, however, much shorter in the present case.

3.4. Decrease of repulsive stresses in GBs

Fig. 10 shows the dislocation source S, emitting four dislocations which pile up against the left GB before their insertion. The distance d_1 between the successive leading dislocations d_i of the pile-up and the GB has been measured as a function of time and source operation, and plotted as a dashed line in Fig. 10h. First, the distance d_i decreases between $\Delta t = 0$ and $\Delta t = 1.92$ s (Fig. 10a and b). Then, the source emits one more dislocation labelled 3 at $\Delta t = 1.96$ s (Fig. 10c). This pushes the top part of the leading dislocation (1) in the GB, thus forming the broad contrast discussed above. The distance d_i is accordingly measured between the second dislocation and the GB ($d_{\mathrm{i}} = d_2$), which corresponds to a steep increase. This distance again decreases, in such a way that the situation at $\Delta t = 6$ s (Fig. 10d) becomes comparable to that at

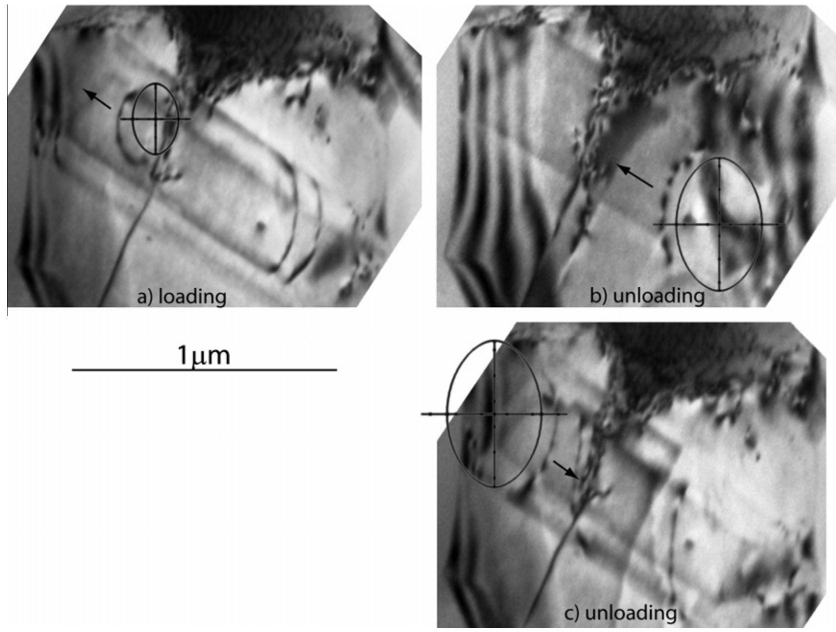

Fig. 8. Local stress measurements during (a) loading and (b and c) unloading. The images are corrected for slip plane inclination, and the curved dislocations are compared with computed loop shapes.

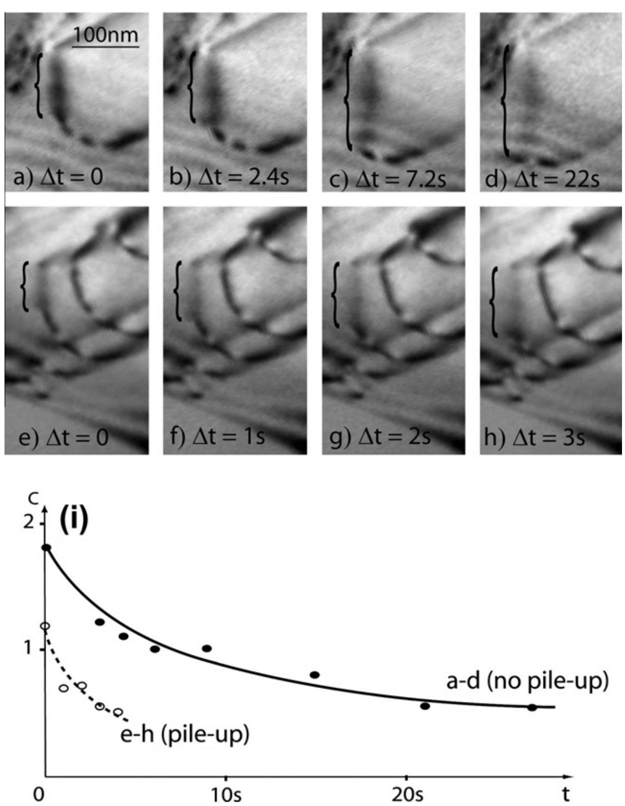

Fig. 9. Contrast of inserted dislocations, as a function of time (same area as Fig. 4). The inserted segments are underlined by brackets. (a–d) Case of an isolated dislocation. (e–h) Case of a dislocation pushed by a small pile-up. (i) The contrast C (in arbitrary units) decreases more rapidly when the forward stress is higher.

$\Delta t = 0$ (Fig. 10a). Then, another dislocation is emitted, and d_2 still decreases until $\Delta t = 9.48$ s (Fig. 10f). Lastly, the second dislocation also enters the GB, which corresponds to $d_i = d_3$. The situation at $\Delta t = 9.54$ s (Fig. 10g) becomes comparable to that at $\Delta t = 2$ s (Fig. 10c).

It is interesting to note that d_2 decreases by a factor of 2 between $\Delta t = 6$ s and $\Delta t = 6.04$ s (Fig. 10d and e), i.e. when the number of piled-up dislocations increases. This can be interpreted by an increase of the pile-up head stress by a factor of 2, i.e. by an increase of the effective number of piled-up dislocations from $N = 1$ to $N = 2$ (this corresponds to a negligible contribution of the small dislocation arm attached to the source).

These data can be used to estimate the repulsion stress of the GB. Considering that the inserted dislocations have the same stress field as an infinitely long dislocation of Burgers vector b_{gb}, the repulsion stress can be expressed as:

$$\tau_{gb} = \alpha \frac{\mu b_{gb}}{2\pi K d} \tag{1}$$

where K depends on the dislocation character ($K = 1$ for a screw, $K = 1 - \nu$ for an edge), and α is a parameter taking into account all the unknown thin foil effects (image forces etc.).

Equating this stress to the pile-up head stress then yields

$$\alpha \frac{\mu b_{gb}}{2\pi K d} = N\tau_f \tag{2}$$

where τ_f is the forward local stress, and

$$b_{gb} = \alpha \frac{N\tau_f}{\mu} 2\pi K d \tag{3}$$

Taking $1/K = 1.35$, $N = 1$ or 2 (see Fig. 10), $\mu = 27$ GPa, and $\tau_f = 45$ MPa, the parameter α is adjusted considering that b_{gb} must increase by the quantity b at each new

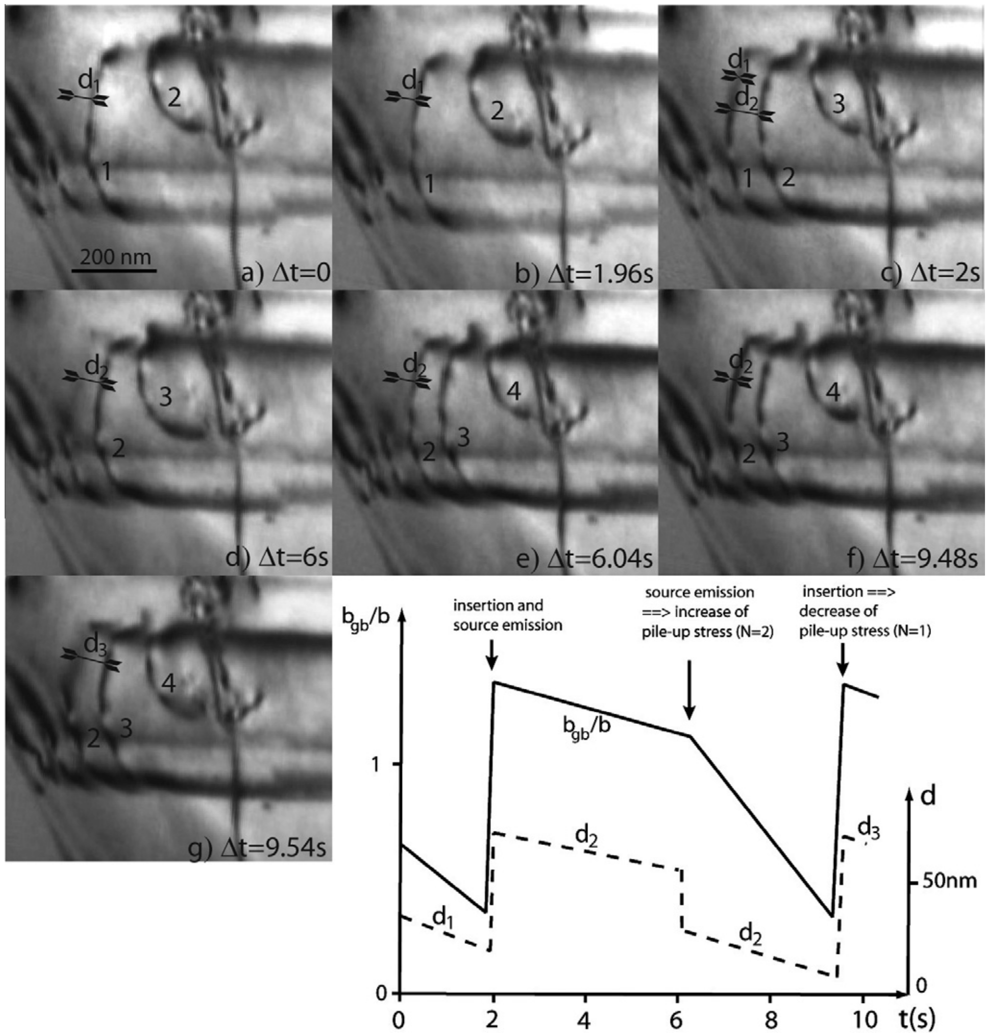

Fig. 10. Direct measurement of the repulsion stress of inserted dislocations. The distance between the GB and the nearest piled-up dislocation is noted d, and the repulsion stress is described by the parameter b_{gb} normalized by the lattice Burgers vector b (see text). Both quantities increase at each new insertion, and progressively decrease with time. Note the faster decrease for the larger forward stress (due to a pile-up effect).

insertion, i.e. at each increase of d by $\Delta d \sim 60$ nm. This yields $\alpha = 2\pi K \Delta d b \mu / \tau_f = 0.78$ and the variation of b_{gb} shown in Fig. 9.

The results are in fair agreement with the contrast measurements of Section 3.3, because:

(i) b_{gb} decreases faster when the stress exerted by the pile-up increases (N increasing from 1 to 2);
(ii) the characteristic times for stress recovery range between 2 s and 14 s, to be compared with the characteristic times for contrast decrease (3.5 s to 9 s).
(iii) This recovery process also explains why up to 33 dislocations can be absorbed in GBs in 36 min, without increasing substantially the flow stress measured at the dislocation source.

For an average value of b_{gb} of the order of b, the back stress is expected to be of the order of 14 MPa at 100 nm from the GB, and 7 MPa at a distance of 200 nm. This can be compared with the direct measurement of a back stress of the order of 20 MPa at 150 nm from the left GBs, in Section 3.2.

3.5. Detailed insertion–extraction process

Fig. 11 is an enlargement of the insertion–extraction process already shown in Fig. 4h. Dislocation 5 ($b = 1/2[0\,1\,1]$) gliding in a $(\bar{1}\,\bar{1}\,1)$ plane intersects the GB which lies in a near-$(\bar{1}\,0\,1)$ plane. The dislocation is partly inside and partly outside the GB (respectively broad contrast 5a and sharp contrast 5b, Fig. 11a). At this moment, and as described schematically in Fig. 11d–g, the segment 5b, which is in screw orientation, cross-slips in the $(1\,\bar{1}\,1)$ plane, in such a way that its extremity in the GB is no more aligned with the inserted segment 5a (Fig. 11b). Then, when the sample is unloaded, at $t = 578$ s (Fig. 11c), the segment 5b pulls another dislocation segment out of the GB instead of the original inserted one. Indeed, this newly extracted

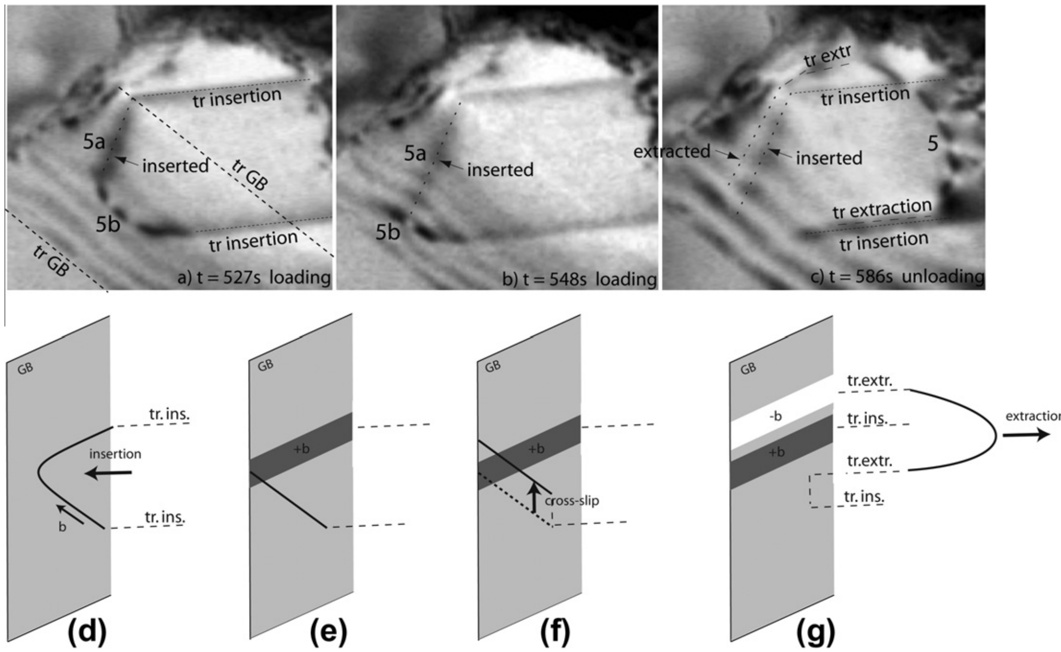

Fig. 11. Detailed sequence of the insertion and extraction of a dislocation, after loading and unloading. (a) The dislocation is partly inserted (in 5a) and partly outside the GB (in 5b), as shown in (d and e). (b) The segment 5b cross-slips, as shown in (f). (c) The segment 5b moves back upon unloading, and extracts a segment which clearly different from the inserted one. As a result of this exchange process, a dipole with a bright-dark contrast is left in the GB, as shown in (g).

segment leaves a bright contrast which is close to, but clearly different from, the dark one at the location of the inserted segment 5a. As a result of this exchange process, the extracted dislocation has glided in a $(\bar{1}\,\bar{1}\,1)$ plane parallel to the incident one, with a slightly shifted slip trace noted "tr extraction". This confirms that the extraction process does not result from the spontaneous recombination of a dislocation spread in a GB, but from the back motion of an external segment pulling out a dislocation which is not necessarily the inserted one. A similar event has already been observed by Balluffi et al. [24].

4. Discussion

The experimental results obtained in the three different grains described above yield an overview of the mechanisms operating during the plastic deformation of UFG aluminium, and upon loading–unloading tests. When discussing dislocation behaviour deduced from observations in thin films, caution is always in place with regard to the validity of such observations with respect to the dislocation behaviour in bulk material. In the present study where the grain size is comparable to (although larger than) the foil thickness, the results obtained were found to conform very satisfactorily to the deformation behaviour previously observed in bulk material, as will be detailed below.

In general, it is found that plasticity is initiated as follows: dislocations are emitted in grains containing sources, and subsequently transferred in adjacent grains. In all cases, they traverse the grains and pile up against the opposite GBs in which they are inserted more or less, as discussed and as already noted in the earlier molecular dynamics study of the deformation of nanocrystals by Schiøtz [25]. Upon unloading, the piled-up dislocations and those that are inserted in the GBs can be released at least partially, giving rise to an appreciable inelastic back flow.

The present observations indicate that dislocation glide is governed by the balanced response of soft and hard zones to the applied stress. If one considers the UFG material as a composite material, consisting of soft and hard zones, as detailed in Ref. [26] for a heterogeneous dislocation distribution, then it follows naturally that soft and hard zones are respectively subjected to backward and forward internal stresses. Now, in a grain containing a source, the pile-up can be considered as the limit between two such zones: (i) the source, which tends to be blocked by the back stress of the pile-up, and which can thus be identified with the soft zone, and (ii) the pile-up head, close to the GBs, which is subjected to the forward pile-up stress, and which can be identified with the hard zone. The exact boundaries of soft and hard zones are difficult to determine precisely. However, since most of the grain is filled by the pile-up, both soft and hard volumes are definitely smaller than the grain volume. Hence, it follows, somewhat surprisingly, that the volume fraction of soft regions need not necessarily be larger than that of the hard regions, as one would perhaps expect intuitively.

The behaviour of grains not containing sources has been less completely investigated, although it also exhibits an inelastic back flow upon unloading, and seems to be ruled by the same mechanisms as in the two other grains (stress concentrations in GBs favouring the extraction of non-fully inserted dislocations). The deformation of grains not containing sources requires the transmission of plastic flow across grain boundaries. This occurs in highly deformed zones where detailed investigations are difficult. For these reasons, the discussion will be focused on the two first grains where dislocations sources started at the very beginning of plastic deformation.

Using Orowan's law, and considering that one or two dislocations move back over the whole grain width upon unloading, the inelastic reverse strain is of the order of 2×10^{-4} to 5×10^{-4} in the second and third grains. This is equivalent to what has been measured in macroscopic tests, which indicates that the inelastic effect was well reproduced in the microsample.

In all cases, and as a result of the small grain size, mobile dislocations are very rapidly absorbed by GBs. Grain boundaries are actually very efficient dislocation sinks, as shown in the second grain, where more than 30 dislocations have been absorbed by two GBs in 36 min. However, as shown in Fig. 5, these repeated absorption processes can generate fairly large stress fields, which contribute to the inelastic back flow.

The inelastic back flow has been observed in two cases:

(i) when dislocations pile up at distances of a few hundreds of nm;
(ii) when dislocations are only partly inserted in GBs.

Then, the repulsive stress of GBs is sufficient to induce the back motion of piled up dislocations in the first case, and to pull back non-inserted segments extracting dislocations from GBs in the second case.

The inelastic back flow has not been observed, when the dislocations emitted by the source are completely inserted in GBs, and when they are dispersed by cross-slip. In the latter case, as observed in Fig. 2, the dislocations enter the GBs at different places, which results in lower stress concentrations. Then, the following dislocations are not significantly repelled; as a result they are completely inserted, and their back motion is impossible.

Short dislocation pile-ups are thus a necessary ingredient to activate a significant back flow upon unloading. In thin microsamples, in which grains are truncated by free surfaces, we can distinguish grains containing near-screw cross-slipping dislocations, which exhibit no reverse back flow (as in Figs. 2 and 3), and grains containing short pile-ups of near-edge dislocations, which exhibit large reverse back flow (as in Figs. 4 and 5). In the bulk UFG material, there is not such a difference because all sources emit both edge and screw dislocations. Then, stress concentrations should always appear in the direction of motion of the edges, and all grains (at least those containing sources) should exhibit back flow.

The key process at the origin of the mechanical properties of UGF materials is undoubtedly the interaction of dislocations with GBs. Dislocations inserted in GBs have a progressively vanishing contrast, but their residual stress field remains present even after long waiting times. According to our observations, the dissolution of inserted dislocations can be described in two steps: (i) a rather short one, with a characteristic time of a few seconds to a few tens of seconds, where those dislocations still behave like ordinary lattice ones; and (ii) a longer one, where the dislocation stress field is mixed with that of all previously inserted ones.

In the first step, inserted dislocations have a broad core, which can be observed under the same contrast conditions as lattice dislocations. Their long-range stress field is similar to that of lattice dislocations with Burgers vector b_{gb} comprising between $1.5b$ and zero. A higher strain rate increases the rate of dislocation insertion (increase of b_{gb}), but also increases the pile-up head stress and thus the rate of recovery (decrease of b_{gb}), in such a way that b_{gb} cannot increase much above b. The stress field of these dislocations is sufficient to repel short dislocation pile-ups, and to induce their back motion when the applied stress is released. For $b_{gb} = b$, it can account for a back stress of the order of 20 MPa at 200 nm from the GBs.

In the second step, inserted dislocations are dissolved in a larger area, which, after enough stress accumulation, appears as a distortion of the GB fringe contrast, or as a broad contrast of 100 nm width (Fig. 5). This stress field is strong enough to form dislocation pile-ups (right GB of Fig. 4), and to extract dislocations when they are only partly inserted, as shown in Fig. 11.

Both kinds of stress fields contribute to the backward stress, which is estimated as 20–23 MPa in the second grain, i.e. half of the forward stress, and one third of the applied stress.

The back stress τ_b acting on dislocation sources in the grain interior can be evaluated considering that it should be of the order of magnitude of the total stress exerted on the pile-up against the source. For a large number N of dislocations in the pile-up of length $D/2$, where D is the grain size, and for a dislocation spacing larger than few atomic distances, the back stress can be estimated as [27]:

$$\tau_b(t) \approx \frac{2\mu b}{\pi(1-\nu)D} N(t) \quad (4)$$

The total number of dislocations in the pile-up varies in time due to (i) the creation of new dislocations, $dN^+(t)$, during the source operation and (ii) the annihilation of dislocations in the GB, $dN^-(t)$, i.e.:

$$dN(t) = dN^+(t) - dN^-(t) \quad (5)$$

The creation term can be written using the Orowan equation as:

$$dN^+(t) = \frac{\dot{\varepsilon} D dt}{b} \quad (6)$$

where $\dot{\varepsilon}$ is the plastic strain rate.

The annihilation term is more complex to estimate because, as shown in Section 3.4, the disappearing time

t_D decreases if a pile-up dislocation closely follows the inserted dislocation. This suggests that the dislocation annihilation is favoured by the elastic field at the head of the pile-up. Since this elastic field depends linearly on N, we thus assume that:

$$dN^{-}(t) = N(t)\frac{dt}{t_D} \tag{7}$$

where t_D is the disappearing time in the absence of pile-up.

Putting Eqs. (6) and (7) into Eqs. (5) and (4) yields:

$$\frac{dN}{dt} = \frac{\dot{\varepsilon}D}{b} - \frac{N}{t_D}$$

whence

$$\tau_{bs}(t) = \frac{2\mu}{\pi(1-\nu)}\dot{\varepsilon}t_D(1-e^{-t/t_D}) \tag{8}$$

The back stress first increases linearly with time and then saturates at

$$\tau_{bs}(t) = \frac{2\mu}{\pi(1-\nu)}\dot{\varepsilon}t_D$$

This behaviour is supported by micro-yielding experiments (Fig. 1) showing the increase and the saturation of the inelastic deformation upon unloading. Taking $\dot{\varepsilon} = 10^{-4}\ \mathrm{s}^{-1}$, $D = 300$ nm, and $t_D = 10$ s, yields $N \sim 1$, in agreement with the present measurements.

The fact that the grain size does not appear in the expression of the back stress results from the assumption that pile-ups with an increasing number of dislocations continue to exist as the grain size increases. Since this is probably not true in large grains (see property (iii) below), Eq. (8) should be valid only in a range limited to grains smaller than 1 μm. On the other hand, in larger grains, Eq. (8) might be valid for just the few leading dislocations which interact directly with the GBs but which are insufficient in number to contribute appreciably to the effects under discussion here.

The observations made in the earlier microyielding studies on UFG copper [4,5] and UFG aluminium [6,7] and in the present in situ TEM investigation indicate that the dislocations generated during loading disappear almost completely during unloading, implying that there is no net increase of dislocation density after a loading/unloading cycle. As already pointed out in our earlier report [14], this matches nicely the results obtained by Van Swygenhoven's group in an in situ X-ray broadening study on tensile-deformed nanocrystalline nickel [28]. In this work, the X-ray peak broadening observed during loading was found to disappear completely during unloading.

Nonetheless, it is not disputed that the variation of grain sizes can also make an additional contribution to the inelastic back flow (and the Bauschinger effect), as concluded by Rajagopalan et al. [8]. However, the effects discussed by these authors are considered to be less important than the effects of dislocation–GB interaction of UFG material, as revealed and elucidated in the present work.

The last point to be discussed is the high inelastic strain in UFG aluminium with respect to that in the CG material. On the basis of the present observations, this can be ascribed to three properties of UFG samples:

(i) Contrary to CG materials, a large amount of dislocations activated during micro-yielding reach GBs and thus build up internal stresses.
(ii) The stress field of inserted dislocations decreases as the inverse of the distance from the GBs. It is thus on average higher in small grains than in large grains, in such a way that the amplitude of back motion can be as large as the grain size only in small grains. The inelastic plastic flow, which is proportional to the ratio of the back motion distance to the grain size, is accordingly higher in UFG materials.
(iii) The dislocation pile-ups are stable only over short distances from the sources, even for near-edge dislocations. For larger slip distances, cross-slip of the screw parts tends to scatter dislocations loops away from their original slip plane, thus reducing the stress concentration at the origin of the inelastic flow.

5. Conclusions

In situ observations of dislocation motion during loading and unloading of UFG Al have yielded the following results:

- During the initial loading procedure, plastic deformation starts in grains where a dislocation source is activated.
- Near-edge dislocations emitted by a source build up high internal stresses, at the intersection of the slip plane and the neighbouring GBs. These internal stresses repel further emitted dislocations, and move them back to the source upon unloading. However, cross-slipping near-screw dislocations reach GBs at different places, leading to a weaker internal stress and less back motion upon unloading.
- A similar behaviour is observed in grains that do not contain sources and which deform by dislocation transfer across the GBs.
- The corresponding inelastic back flow during unloading after microyielding is explicable by the dislocations mechanisms described above and is of the same order as that measured in bulk samples [4–7].
- The dislocation–GB interaction at the origin of the backward internal stress has the following properties:
- Dislocations inserted in GBs have a broad contrast, with a lifetime of a few tens of seconds. The corresponding long-range elastic stress field decreases at the same rate. Both quantities decrease more rapidly at a pile-up head, where the local forward stress is higher.

- Dislocations fully inserted in GBs remain immobile upon unloading. On the contrary, dislocations piled up in front of GBs can move back and annihilate at sources. Dislocations only partly inserted in GBs can also escape and move back, leaving dipolar defects in the GBs.

On the basis of these observations, the formation and the evolution of internal stresses responsible for inelastic back flow have been modelled. The higher back flow in UFG samples with respect to CG material is a direct consequence of the shorter dislocation mean free path, which induces:

- a more rapid stress concentration at GBs, immediately after yielding;
- a higher stress concentration at GBs, due to a weaker scattering of pile-ups by cross-slip;
- a more efficient internal stress for inelastic back strain, because dislocations can move back over distances equal to the grain size.

References

[1] Valiev RZ, Islamgaliev RK, Alexandrov IV. Prog Mater Sci 2000;45:103–89.
[2] Meyers MA. Prog Mater Sci 2006;5:427–556.
[3] Valiev RZ, Estrin Y, Horita Z, Langdon TG, Zehetbauer MJ, Zhu YT. JOM 2006;58:33–9.
[4] Höppel HW, Xu C, Kautz M, Barta-Schreiber N, Langdon TG. Mughrabi H. In: Zehetbauer M, Valiev RZ, editors. Proceedings of second international conference on nanomaterials by severe plastic deformation, NANOSPD2. Weinhein: Wiley-VCH; 2002. p. 677–83.
[5] Mughrabi H, Höppel HW, Kautz M, Valiev RZ. Z Metallkd 2003;94:1079–83.
[6] Mughrabi H, Höppel HW. Kautz M. In: Zhu YT, Varyukhin V, editors. Proceedings of NATO ARW on nanomaterials by high-pressure severe plastic deformation. Berlin: Springer Verlag; 2004. p. 209–16.
[7] Höppel HW, Kautz M, Murashkin M, Langdon TG, Valiev RZ, Mughrabi H. Int J Fatigue 2006;28:1001–10.
[8] Rajagopalan J, Rentenberger C, Karnthaler HP, Dehm G, Saif MTA. Acta Mater 2010;58:4772.
[9] Mompiou F, Legros M, Caillard D, Mughrabi H. J Phys: Conf Ser 2010;240:012137.
[10] Caillard D, Martin JL. Acta Metall 1982;30:791–8.
[11] Caillard D. Acta Metall 1984;32:1484–91.
[12] Priester L. Interf Sci 1997;4:205.
[13] Michaud H, Baillin X, Pélissier J, Putaux JL, Thibault J. Microsc Microanal Microstruct 1993;4:221.
[14] Poulat S, Décamps B, Priester L. Phil Mag A 1999;79:2655.
[15] Couzinié JP, Décamps B, Boulanger L, Priester L. Mater Sci Eng A 2005;400–401:264.
[16] Chassagne M, Legros M, Rodney D. Acta Mater 2011;59:1456.
[17] Pettinari F, Couret A, Caillard D, Molénat G, Clément N, Coujou A. J Microscopy 2001;203:47.
[18] Douin J, Veyssière P, Beauchamp P. Phil Mag A 1986;54:375.
[19] Pumphreys PH, Gleiter H. Phil Mag 1974;30:593.
[20] Varin RA. Phys Stat Sol (a) 1979;52:347.
[21] Valiev RZ, Gertsman UYu, Kaibyshev DA. Phys Stat Sol (a) 1983;78:177.
[22] Swiatnicki WA, Lojkowski W, Grabsli MW. Acta Met 1986;34:599.
[23] Kwiecinski J, Wyrzykowski JW. Acta Met 1989;37:1503.
[24] Balluffi RW, Komen Y, Shober T. Surf Sci 1972;31:68.
[25] Schiøtz J. Scripta mater 2004;51:837–41.
[26] Mughrabi H. Acta Metall 1983;31:1367.
[27] Eshelby JD, Franck FC, Nabarro FRN. Phil Mag 1951;42:351.
[28] Budrovic Z, Van Swygenhoven H, Derlet PM, Van Petegem S, Schmitt B. Science 2004;304:273–6.